Deposition, characterization and high-temperature steam oxidation behavior of single-phase Ti_2AlC-coated Zircaloy-4

Chongchong Tang[a]*, Martin Steinbrueck[a], Michael Stueber[a], Mirco Grosse[a], Xiaojuan Yu[b], Sven Ulrich[a], Hans Juergen Seifert[a]

[a]*Institute for Applied Materials (IAM), Karlsruhe Institute of Technology (KIT), D-76021 Karlsruhe, Germany*
[b]*Institute for Functional Interfaces (IFG), Karlsruhe Institute of Technology (KIT), D-76021 Karlsruhe, Germany*

Corresponding author: Chongchong Tang

Email: chongchong.tang@kit.edu

Abstract: Oxidation of single-phase and dense Ti_2AlC coatings with or without a 500 nm TiC diffusion barrier deposited on Zircaloy-4 by annealing of nanoscale multilayer stacks between 800°C and 1200°C in high-temperature steam was investigated. Coatings without TiC barrier formed a duplex scale: outer θ-Al_2O_3 rich layer mixed with TiO_2 and inner porous TiO_2 layer; correspondingly, a triple-layered scale (θ-Al_2O_3+TiO_2/θ-Al_2O_3/TiO_2) grew on coatings with barrier at 800°C. The TiC barrier suppresses the rapid diffusion of Al into the substrate, contributing to improved performance and longer life of Ti_2AlC/TiC coatings. However, both coatings demonstrated low protection effect from 1000°C in steam.

Key words: A. Sputtered films

A. Zirconium

B. SEM

C. High temperature corrosion

C. Oxidation

1. Introduction

Nuclear power provides around 13% of the world's electricity with over 400 nuclear reactors in operation worldwide. The majority of these reactors are water-cooled reactors [1]. Zirconium-based alloys, like Zircaloy-4 and M5®, are currently utilized as fuel cladding and structural components in these commercial reactors due to their low thermal neutron absorption cross section, good mechanical properties and reasonable corrosion resistance during operation conditions [2]. In general, the corrosion of the cladding by coolant water results in initial formation of a dense, adherent oxide layer following a cubic rate growth law. Once the oxide layer exceeds a certain critical thickness, fracture of the oxide layer takes place, leading to a large amount of cracks in the oxide. The growth kinetics transforms to a linear law with accelerated corrosion rate [3]. Moreover, hydrogen generated by the corrosion reaction between zirconium and water can be absorbed by the cladding and eventually precipitate as hydrides, leading to the hydride embrittlement of the cladding. Hydride formation can strongly degrade the cladding performance during design-basis (DB) and beyond design-basis (BDB) accident scenarios [3]. One additional undesirable feature of zirconium-based cladding is their extremely fast oxidation kinetics with high-temperature steam during loss of cooling accidents (LOCA) [4]. A considerable amount of heat and hydrogen gas is produced by the reaction of zirconium and steam. The heat generated by the steam oxidation reaction becomes comparable to or even exceeding the decay heat. In a serious situation, like station blackout (SBO), the core suffers severe degradation and hydrogen explosion can occur, followed by subsequent release of highly-radioactive fission products to the environment like during the nuclear accidents at the Fukushima Daiichi Nuclear Power Plant in 2011 [5].

The concept of accident tolerant fuels (ATF) moved into the focus of international research after Fukushima, aiming at providing substantially improved safety margins and increasing coping time during severe accidents while maintaining the fuel performance under normal operating conditions [6]. Different strategies are being investigated. One approach is to develop oxidation resistant bulk materials, like SiC-based composite, FeCrAl alloys, and triplex molybdenum cladding replacing current zirconium-based alloy claddings [6–8]. An alternative strategy is the protection of state-of-the-art zirconium-based alloy fuel claddings with an oxidation resistant coating. This solution promises the elimination of the hydrogen pickup during normal operation, as well as significant improvement of the reaction kinetics with steam during off-normal conditions. Different types of coating materials, mainly TiO_2-, Al_2O_3- or Cr_2O_3- forming, are being investigated [9–13].

$M_{n+1}AX_n$ (or MAX) phases, where M is an early transition metal, A is an A-group, mostly groups IIIA and IVA, element and X is either C and/or N, n=1-3, represent hexagonal carbides and nitrides consisting of a nanolaminated structure [14]. These compounds combine many attractive properties of both ceramics and metals, such as lightweight, machinability, damage tolerance and thermal shock resistance, as well as excellent thermal conductivity. Al-containing MAX phases, like Ti_2AlC, Ti_3AlC_2, Cr_2AlC, are promising coating materials because of their excellent high-temperature oxidation resistance both in air and steam, self-healing in an oxygen-containing service environment as well as with outstanding mechanical properties and irradiation stability [15–18]. In previous studies relatively thick (dozens of micrometers) Ti_2AlC coatings were deposited on zirconium-based alloys by cold spray [19] or high velocity oxy-fuel (HVOF) [20]. Therefore, the structure of the coatings was loose consisting of large amount of TiC and/or TiAl intermetallic secondary phases. These phases have been proved to reduce the oxidation resistance of the Ti_2AlC materials. Yeom et al. recently deposited Ti_2AlC coatings on Zircaloy-4 substrate by dc magnetron sputtering with following laser surface annealing at 900°C in order to maintain the substrate microstructure. However, formation of micro-cracks was observed within the coatings after surface annealing [21].

In our previous study, an elemental nano-multilayer stack deposited by non-reactive magnetron sputtering followed by *ex-situ* annealing was adopted to prepare Ti_2AlC coatings. The microstructural evolution of the coatings during *ex-situ* annealing from 600°C to 900°C was systematically investigated and the results demonstrated that phase-pure, i.e. single-phase polycrystalline Ti_2AlC coatings on SiO_2/Si were obtained after 800°C annealing in argon for 10 min [22]. This work attempted to synthesize the phase-pure polycrystalline Ti_2AlC MAX phase coatings on polished Zircaloy-4 substrates by the same approach using non-reactive magnetron sputtering of elemental multilayer thin films with a multiple stacking sequence of titanium, -carbon, and -aluminum layers from three element targets, and subsequent thermal annealing in argon at 800°C. The overall coating thickness was around 5.5 μm with or without a 500 nm thickness TiC diffusion barrier. Single-phase and dense Ti_2AlC coatings were obtained after annealing at 800°C below the phase transformation temperature of Zircaloy-4 substrates. The microstructure, adhesion and mechanical properties of the coatings were evaluated using X-ray diffraction, scanning electron microscopy, Raman spectroscopy, hardness test and scratch test methods. The performance of the coatings in high-temperature steam from 800°C to 1200°C was examined and compared to bare Zircaloy-4 samples and bulk Ti_2AlC ceramic.

2. Material and methods

Square Zircaloy-4 (Zry-4) alloy specimens (~10 × 10 × 0.60 mm^3) cut from a large plate were used as substrates in the present study. The chemical composition (wt.%) of the Zircaloy-4 was as follows: Sn ~1.4, Cr ~0.10, Fe ~0.22, O ~1000 ppm, Zr bal. The specimens were firstly ground with SiC paper, followed by polishing using diamond paste, and finally rinsed with active oxide polishing suspensions and water. The finished surface roughness (Ra) was around 50 nm. An elemental nanoscale multilayer approach was used to prepare the Ti_2AlC MAX phase coatings. Fig.1 shows the schematic of the design of the multilayer system. The multilayer stacks were deposited by non-reactive magnetron sputtering using a laboratory Leybold Z 550 coater from three elemental targets. The periodical stack (with a thickness of ~14 nm) has been repeated until a desired total film thickness was obtained. The overall coating thickness was around 5.5 μm (Fig.1a). For one batch of coatings, a 500 nm thick Ti-C multilayer was deposited as diffusion barrier (Fig.1b). The substrates were ultrasonically cleaned in acetone bath for 10 min before being introduced into the deposition chamber. The base pressure was around 1×10^{-4} Pa and the working pressure of the Ar gas during deposition was kept at 0.5 Pa, respectively. The substrates were plasma-etched with R.F. power of 500 W for 15 min prior to deposition. All three targets were at a target power of 200 W, R.F. for titanium and aluminum targets and D.C. for carbon target. During deposition, the PVD facility ran in a stop-and-go mode, and the overall deposition rate was around 1 μm per hour. Only the two main sides of the substrates were coated. For detailed information on the synthesis of the coatings, please refer to reference [22].

After deposition, the coatings were *ex-situ* annealed in pure Ar (99.9999%) at 800°C for 10 min using a commercial thermal balance (NETZSCH STA-449) to yield the formation of Ti_2AlC MAX phase. The heating and the cooling rates were fixed at 10 K/min. The composition of the as-deposited coatings was measured by electron probe microanalysis (EPMA) with a Cameca microbeam system. An average value based on four measurements located in different regions was taken. The crystalline structures of the coatings, including the as-deposited and annealed, was analyzed by X-ray diffraction (XRD, Seifert PAD II diffractometer), and Raman spectroscopy (Renishaw Raman 1000). The XRD signals were collected in Bragg–Brentano geometry with CuKα radiation (λ= 1.54Å) at a voltage of 40 kV and a current of 30 mA. The Raman spectra were collected and recorded between 160 and 2000 cm^{-1} using an Argon-ion laser with wavelength 514.5 nm and power 2~3 mW. The indentation hardness and reduced Young's modulus of the coatings were measured with a Berkovich nano-indenter (UMIS 2000). During the indentation test, the indentation depth was adjusted to be significantly higher than the surface roughness but less than 1/10 of the total film thickness to avoid substrate effects. The values

reported herein represent the average based on at least ten indentations per sample. The coating-substrate adherence was evaluated by scratch tests (CSM Revetest) applying an increasing load of 20 N/cm up to 80 N and further determination of the critical load from the micrographs of the scratches. The scratch tests were repeated for three times to obtain an average and accurate results.

The performance of the coatings in high-temperature steam from 800°C to 1200°C was examined also using the NETZSCH STA-449 thermal balance with a steam furnace. The bare Zircaloy-4 samples and a commercial Maxthal 211® bulk ceramic (nominally Ti_2AlC, Kanthal/Sweden) were tested at the same conditions for comparison. After oxidation, the surface oxide scale was characterized by XRD using the same setup as before. The surface and cross-section microstructures were analyzed by an optical microscope (OM, Reichert-Jung MeF), as well as by a field-emission scanning electron microscope (SEM, Philips XL30S) equipped with an energy dispersive X-ray spectroscopy (EDS) detector for element analysis. For cross-sectional examination, the samples were firstly embedded in epoxy resin, then ground using SiC paper from 800 down to 2400, and finally polished with a sequence of 15, 6 and 3 μm diamond pastes. The surfaces of coated Zry-4 samples after oxidation at 800°C for 5 min were additionally examined by X-ray photoelectron spectroscopy (XPS). The measurements have been carried out using an IR/XPS–UHV system (Prevac) equipped with a VG Scienta R4000 electron energy analyzer. A monochromatic Al Kα X-ray source (1486.6 eV) was used as incident radiation. The energy scale has been calibrated to the reference peaks Au4f7/2 (84.00 eV) and Ag3d5/2 (368.26 eV). Prior to the data acquisition, the surface was sputtering etched using Ar^+ ion (1.5 keV, 10 mA) for around 5 mins to remove residual surface contamination. A CasaXPS Processing Software was used to treat the XPS spectra with a mixed Gaussian-Lorentzian function and Shirley background subtraction.

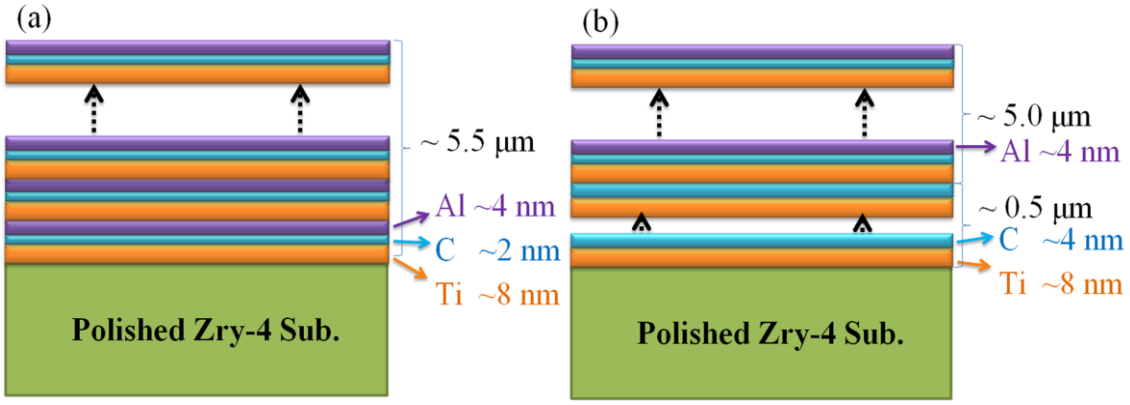

Fig.1 Schematic of the elemental nanoscale multilayer stacks on polished Zry-4 substrates. (a) without Ti-C barrier, (b) with around 500 nm thick Ti-C barrier.

3. Results

3.1. Characterization of the coatings

3.1.1. Composition and structure

The chemical composition of the as-deposited Ti-C-Al coatings without Ti-C diffusion barrier determined by EPMA was 50.49 ± 0.16 % Ti, 22.74± 0.40 % C and 26.77 ± 0.31 % Al (at.%). The results demonstrated that the composition of the as-deposited coatings was close to theoretical stoichiometry of the Ti_2AlC MAX phase. Fig.2 shows the XRD patterns of the as-deposited Ti-C-Al coating and Ti_2AlC coatings with and without TiC barrier after annealing at 800°C for 10 min in argon. Apart from the diffraction generated by the Zry-4 substrates, only one broad diffraction signal located at around 38° was observed which was indexed as a combination of Ti(110) (PDF card No. 44-1294) and Al(111) (PDF card No. 04-0787) planes as shown in diffractogram (a) in Fig.2. This finding indicated that the titanium and aluminum layers consisted of nanocrystalline grains with relatively low crystallinity and the carbon layers, as expected, were grown in amorphous state in the as-deposited coatings. After annealing, the XRD patterns displayed different features. The clearly visible signals at 2θ= 12.98º and 39.52º can be assigned to Ti_2AlC (002) and (006) planes (PDF card No. 29-0095). The absence of common competing phases, like TiC, Ti_3AlC, Ti_3AlC_2 and Ti-Al intermetallics during the growth of Ti_2AlC coatings, was confirmed by Fig.2b for the coatings without TiC diffusion barrier after annealing. For the coating with Ti-C barrier, additional diffractions belonging to the TiC phase were distinguished after annealing (Fig.2c). The broader peak located at around 36.08 º corresponded to the TiC (111) (PDF card No. 32-1383) plane. Therefore, it can be claimed that the Ti-C and Ti-C-Al elemental multilayer stacks have transformed to corresponding TiC and Ti_2AlC phases after annealing at 800°C for 10 min. The grain size of the Ti_2AlC MAX phase coatings after annealing was calculated based on the Scherrer's equation using the XRD peaks. The results suggested the grain size were in the range of 15 - 20 nm, consistent with a previous study determined by TEM [22].

Raman spectroscopy analyses were performed to identify the microstructure evolution before and after annealing as it represented a sensitive tool for carbon-containing materials. Fig.3 shows the Raman spectra recorded in the range of 160-2000 cm^{-1} of the as-deposited Ti-C-Al coatings and the annealed coatings with and without TiC barrier. The Raman active modes of 211 MAX phases have been well addressed. There are 4 Raman active optical modes for 211 structures, and all Raman active frequencies are located in the low wave-number region [23]. Concerning the Ti_2AlC MAX phase, the calculated Raman vibration modes of E_{1g}&E_{2g} and A_{1g} are located at 266

and 358 cm^{-1} [24]. The Raman active frequencies of materials containing amorphous carbon have two typical modes, the D band at around 1350 cm^{-1} and the G band at around 1580-1600 cm^{-1} [25]. Curve (a) in Fig.3 demonstrated that there were no distinguishing sharp peaks except one broad hump corresponding to D and G bands in the spectrum of as-deposited Ti-C-Al coatings. In consistence with the XRD findings, this suggested that the carbon layers were amorphous in the coatings. For coatings without Ti-C barrier after annealing at 800°C, the Raman active modes attributed to Ti_2AlC were clearly seen as shown in Fig.3b. The peaks of E_{1g}&E_{2g} and A_{1g} modes are located at 265.7 and 361.8 cm^{-1}, respectively, which agreed quite well with the theoretical values. The peaks were sharp with high intensity, indicating that the coating was well-crystallized after annealing. The broad peak located at the region of 500-750 cm^{-1} was caused by a thin oxide layer formed on the surface of coatings during annealing due to residual oxygen in the furnace. The same phenomenon has been observed during the annealing of amorphous Cr-C-Al thin films [26]. Furthermore, no signals were detected in the region of D and G bands. The findings confirmed that phase-pure Ti_2AlC coating was obtained after 800°C annealing. Apart from the vibration modes of Ti_2AlC, the coating with Ti-C barrier in addition showed the peaks belonging to the TiC phase, i.e. the 200.0 cm^{-1}, the D and G modes, after annealing. Stoichiometric TiC had been confirmed to possess no Raman active frequencies; hence, these peaks demonstrated that the Ti-C layer changed to hypo-stoichiometric TiC_x (x<1) [27]. This was reasonable because the density of deposited carbon layer was usually lower than the theoretical density of the graphite target [28], which was adopted herein to calculate the thickness of the carbon nanolayer required.

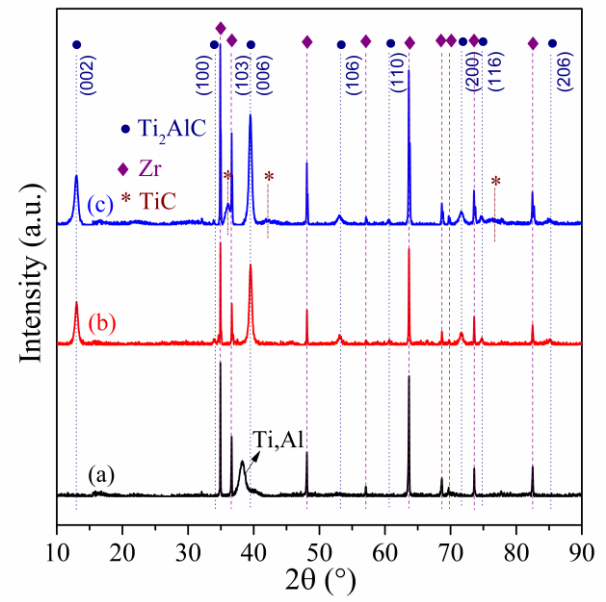

Fig.2 XRD patterns of coatings on Zry-4 substrates. (a) as-deposited Ti-C-Al coating, 800°C annealed coatings (b) without and (c) with Ti-C barrier after annealing.

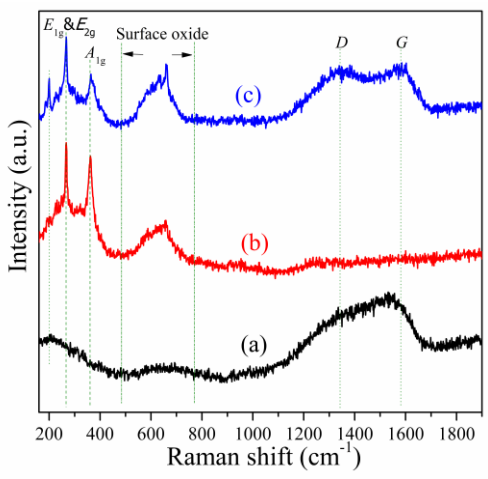

Fig.3 Raman spectra of coatings on Zry-4 substrates. (a) as-deposited Ti-C-Al coating, 800°C annealed coatings (b) without and (c) with Ti-C barrier after annealing.

Fig.4 shows the SEM images of the surface and cross section together with elemental X-ray mapping of the coatings after 800°C annealing. As shown in Fig.4, the coating was uniform, dense and free of voids and micro-cracks in this scale. The Ti_2AlC coating and TiC barrier layer can be easily distinguished and the thickness of the coating was consistent with the predicted values based on measured deposition rates. Diffusion of Al from the coating into the Zry-4 substrate was observed for the coating without the TiC barrier and the thickness of the diffusion layer was around several hundred nanometers as identified by EDS-mapping (Fig.4b'). The TiC layer can effectively prevent the fast outward diffusion of Al into the substrate as no apparent diffusion layer at the interfaces was observed as shown in Fig.4b.

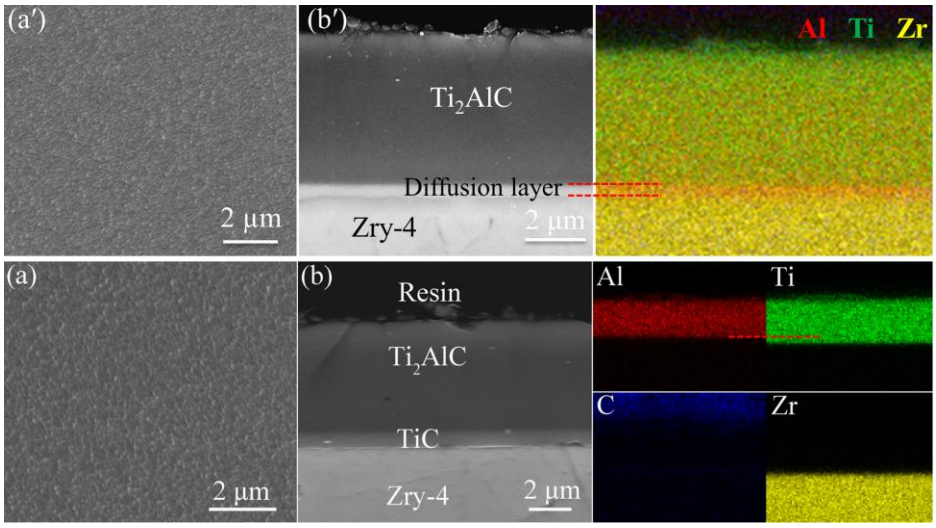

Fig.4 SEM images of surface top view and cross section view with EDS elemental mapping of the coatings on Zry-4 after 800°C annealing. (a') and (b') Ti_2AlC coating, (a) and (b) Ti_2AlC coating with TiC barrier.

3.1.2. Mechanical properties

Fig.5 shows the hardness and reduced Young's modulus with the standard deviation of the substrate with and without coatings. The Zry-4 substrate was proved to be relatively soft, and the indentation hardness and reduced Young's modulus were 2.8 ± 0.2 GPa and 70.1 ± 7.1 GPa, respectively. The findings are similar and consistent with previously reported values, which are in the range of 2-3 GPa for hardness and ~ 100 GPa for Young's modulus of Zircaloy-4 cladding [29]. The coatings, both the as-deposited and the annealed, as typical composite or ceramic materials were much stiffer than the Zry-4 substrate. The coatings with and without TiC diffusion barrier had similar values; the indentation hardness and reduced Young's modulus of the as-deposited coatings were about 8.5 GPa and 120 GPa, respectively. After annealing, both the hardness and modulus roughly doubled, around 15 GPa for hardness and 200 GPa for modulus. The tendency and values were in accordance with the previous studies [22].

Fig.6a displays the surface morphology SEM images of the coatings after scratch tests and Fig.6b shows the critical load when the coatings failed during the test. The critical load is defined as the coatings lost and the substrate becomes continuously visible (L_{C2}), i.e. the average minimum value with occurring spallation of the coatings. Significant tensile cracking was observed both for the coatings with and without barrier around the initial failure area. Once the load exceeded the critical load, extensive spallation and delamination of the coatings were observed, demonstrating a brittle failure mode. This could be expected due to the natural brittleness of ceramic materials. The average critical load of the Ti_2AlC coating without TiC barrier was about 50 N, around 20 N higher than that of Ti_2Al/TiC coating (Fig.6b). The fast diffusion of Al into the substrate resulted in the formation of a strong metallurgical bond at the coating/substrate interface (Fig.4b'), increasing the interfacial adhesion of the Ti_2AlC coatings without diffusion barrier.

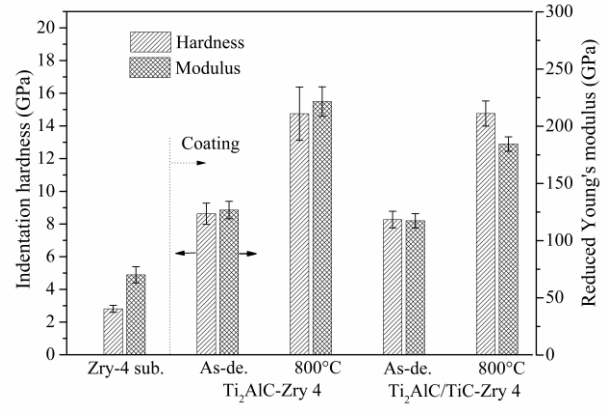

Fig.5 Indentation hardness and reduced Young's modulus of Zry-4 substrate, with and without coatings.

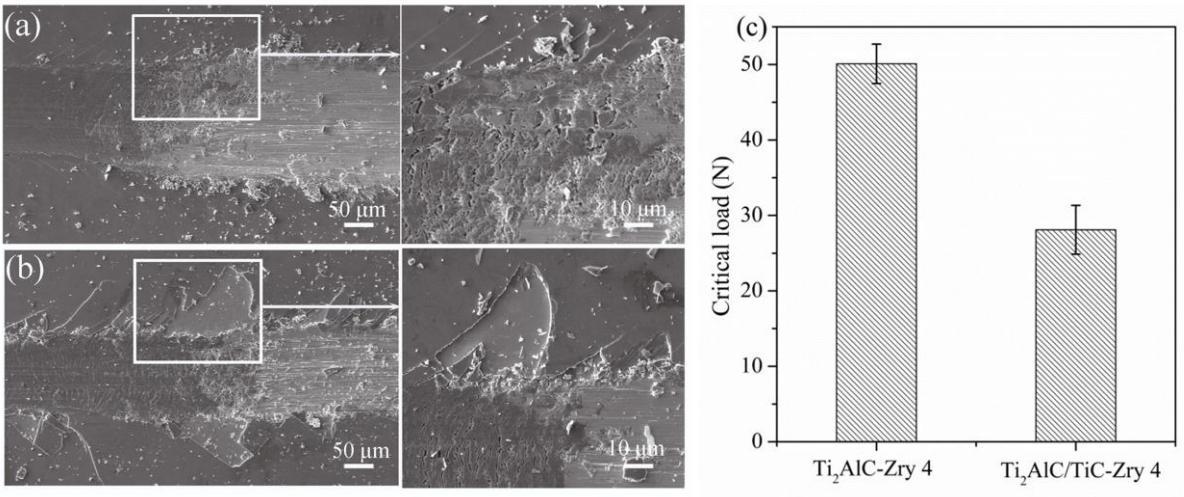

Fig.6 Scratch test of Ti_2AlC- and Ti_2AlC/TiC-coated Zry-4 after annealing. SEM images of surface view (a) Ti_2AlC coating and (b) Ti_2AlC/TiC coating after scratch, (c) critical load when the coatings fail.

3.2. High-temperature oxidation behavior in steam

Isothermal oxidation tests from 800 to 1200°C of bare and coated Zry-4 along with Ti_2AlC bulk ceramic and ramp tests from 300 to 1000°C with 10 K/min heating rate of bare and coated Zry-4 in steam were conducted to investigate the oxidation behavior of the coatings and to compare the coatings and the bulk materials.

Fig.7 presents the general post-test appearance of the coated samples after isothermal oxidation in steam at 800°C for 5 and 250 min, 1000°C for 5 min, and 1200°C for 15 min, respectively. It could be distinguished that 800°C - 5 min oxidation of Ti_2AlC-coated Zry-4 and 800°C - 5 and - 250 min oxidation of Ti_2AlC/TiC-coated Zry-4 had not fully consumed the coatings, whereas all other coatings were completely oxidized. The Ti_2AlC coatings with TiC barrier demonstrated obvious better oxidation resistance than those of without barrier. The uncovered edges oxidized much faster as shown in the 800°C- 250 min oxidation of Ti_2AlC/TiC-coated Zry-4 sample. The coatings were quickly consumed, even with just 5 min oxidation, once the temperature reached or exceeded 1000°C as shown in the Fig.7. Widespread cracks, spallation and delamination were observed for the fully oxidized coatings.

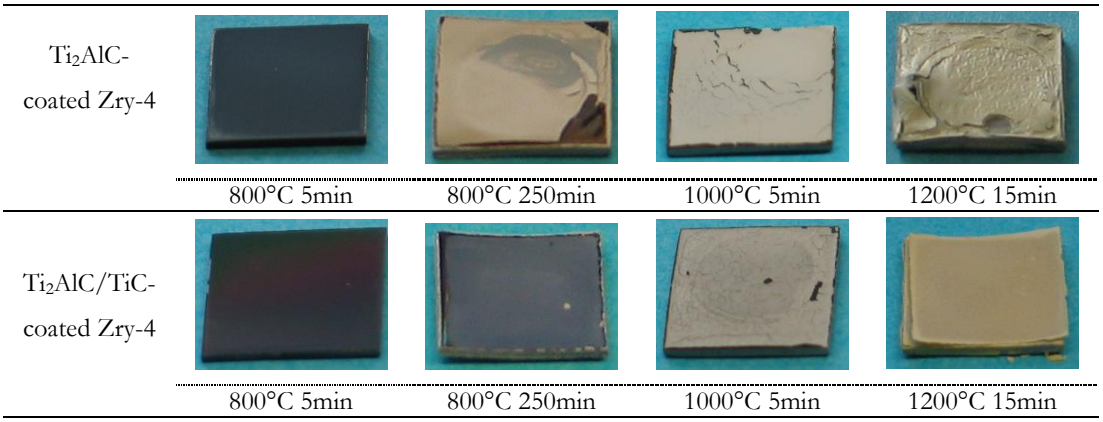

Fig.7 Post-test appearance of the samples after isothermal oxidation in steam at different temperatures and times.

3.2.1. 800°C oxidation

Fig.8 shows the oxidation kinetics, i.e. weight gain per unit area as a function of exposure time, of the polished Zry-4 substrate, Ti_2AlC- and Ti_2AlC/TiC-coated Zry-4 and bulk Ti_2AlC at 800°C up to 250 min in steam. The dashed lines displayed the fitting results of the weight gain versus oxidation time curves using two different oxidation rate laws, i.e. cubic and parabolic, within selective time interval. Generally, the oxidation kinetics of uncoated Zry-4 obeyed a cubic law during the whole exposure up to 250 min. Parabolic kinetics were found for the coated Zry-4 during initial oxidation and for the bulk Ti_2AlC ceramic. The mass gain of the coated Zry-4 was significant lower during the initial stage of exposure compared to uncoated samples. The Ti_2AlC/TiC-coated Zry-4 exhibited very similar mass gain to bulk Ti_2AlC up to around 150 min. However, the oxidation of Ti_2AlC-coated Zry-4 was about two times faster than that of Ti_2AlC/TiC-coated Zry-4 before the exposure time reaching 100 min. Transformation of the oxidation kinetics to much faster rate was observed for both coatings with and without barrier as shown by the fitting dashed lines. The transformation time was significantly shorter and the oxidation rate after the transformation point was obviously faster for Ti_2AlC-coated Zry-4 than for that with TiC barrier. This difference is caused by the quick consumption of the coatings without TiC barrier exposing the fresh surface of the substrates and faster oxidation of the uncovered edges of the samples with TiC barrier, respectively, which will be explained later. The Ti_2AlC/TiC coated Zry-4 showed significantly improved oxidation resistance during oxidation at 800°C for 250 min in steam with several times lower mass gain than that of bare Zry-4.

The XRD patterns of oxide scales formed on the surface of coated Zry-4 substrates after 800°C steam oxidation for different times are shown in Fig.9. The evolution of different phases

with increasing oxidation time can be found. The diffractions originated from the substrate (Zr) and un-reacted Ti_2AlC were clearly seen after 5 and 70 min oxidation for Ti_2AlC coatings and 5 and 250 min oxidation for Ti_2AlC/TiC coatings. The intensity of these two phases in the Ti_2AlC/TiC coatings was apparently stronger than that of Ti_2AlC coatings, showing faster oxidation rate for the coatings without TiC barrier. Two different oxidation products were detected: rutile (TiO_2) and metastable alumina (θ-Al_2O_3). The intensities of diffraction peaks correlated to rutile increased considerably for the Ti_2AlC/TiC coatings with oxidation time increasing from 5 to 250 min. The ZrO_2 phase was observed after 250 min oxidation of Ti_2AlC coatings due to the complete consumption of the coating followed by spallation.

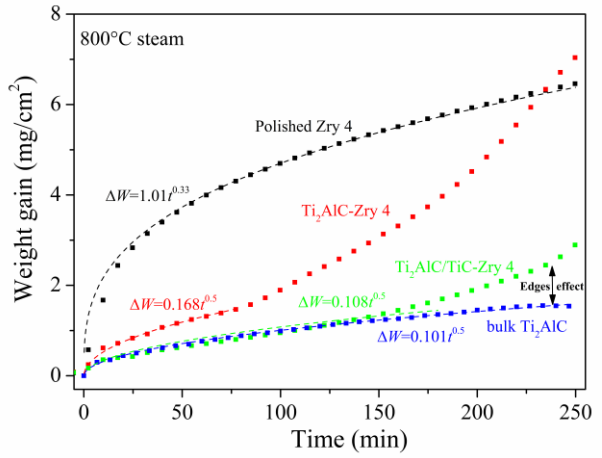

Fig.8 Oxidation kinetics of bulk Ti_2AlC, polished Zry-4 substrates, and Ti_2AlC- and Ti_2AlC/TiC-coated Zry-4 at 800°C in steam.

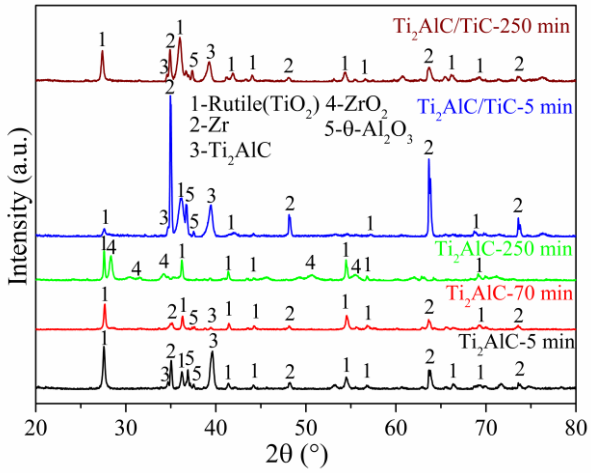

Fig.9 X-ray diffraction patterns of oxide scales formed on the surface of Ti_2AlC- and Ti_2AlC/TiC-coated Zry-4 substrates after 800°C steam oxidation at different times.

Fig.10 shows the SEM images of typical surface morphologies of Ti_2AlC- and Ti_2AlC/TiC-coated Zry-4 together with bulk Ti_2AlC after oxidation at 800°C in steam. The surface morphologies were similar for the coated samples after short time oxidation (Fig.10a and d) and

evolution of the surface morphologies was observed over oxidation time. Two different types of grains, fine whiskers and angular plates, were observed for the three samples, and the volume content of each type of grains changed with the oxidation time. Based on the XRD results and previous studies [30,31], the whisker and angular plate grains can be identified as θ-Al_2O_3 and rutile, respectively. The volume content of both grains, especially whisker grains, on the surface of Ti_2AlC coatings (Fig.10a) were much higher than that on Ti_2AlC/TiC coatings (Fig.10d) after oxidation for 5 min. After 70 min oxidation of the Ti_2AlC coating, the surface was rich in whisker θ-Al_2O_3 grains as shown in Fig.10b. The Ti_2AlC coating, which was fully oxidized after oxidation for 250 min, partially spalled off and the Zircaloy-4 substrate was exposed with relatively smooth surface and granular grains (Fig.10c). On the contrary, the Ti_2AlC/TiC coating persisted adhesive after 250 min oxidation and the growth of whisker θ-Al_2O_3 grains to slightly bigger size was shown (Fig.10e). Concerning the bulk Ti_2AlC, it could be clearly seen that the grain size of the θ-Al_2O_3 and rutile formed on the surface was considerably smaller than that on the coatings. The coatings retained its integrity without spallation or formation of cracks before being completely oxidized; however, the surface oxide layer was porous and some voids and pores existed.

In order to further confirm the oxidation products on the surface of the coatings, XPS measurements were conducted for the coatings after oxidation at 800°C for 5 min. XPS is a surface analysis tool which is very sensitive to the chemical compositions and environments of atoms. The spectra of Ti, Al and C of Ti_2AlC/TiC coatings are displayed in Fig.11. Two different states of Ti and Al were found, corresponding to the oxidation products and the beneath Ti_2AlC coating (Fig.11a and b). The Ti $2p_{2/3}$ and Al 2p peaks in the oxide were located at around 458.8 eV and 73.8 eV, respectively, identified as rutile (R-TiO_2) and metastable θ-Al_2O_3 compared with the values reported before [32]. The absence of Anatase (A-TiO_2) and α-Al_2O_3 is coincident with previous reports, i.e. one is stable at low temperature (< 700°C) and the other one usually starts to grow beyond 900°C [30]. Therefore, the O1s band could be decomposed into two parts, the peak at 530.0 eV for rutile and at 530.8 eV for θ-Al_2O_3 (Fig.11c). The intensity raised by the O and Al in alumina was several times higher than that of O and Ti in rutile. The observations indicated that the surface was composed of a mixture of rutile and θ-Al_2O_3 with the θ-Al_2O_3 acting as the main component at the initial stage of oxidation.

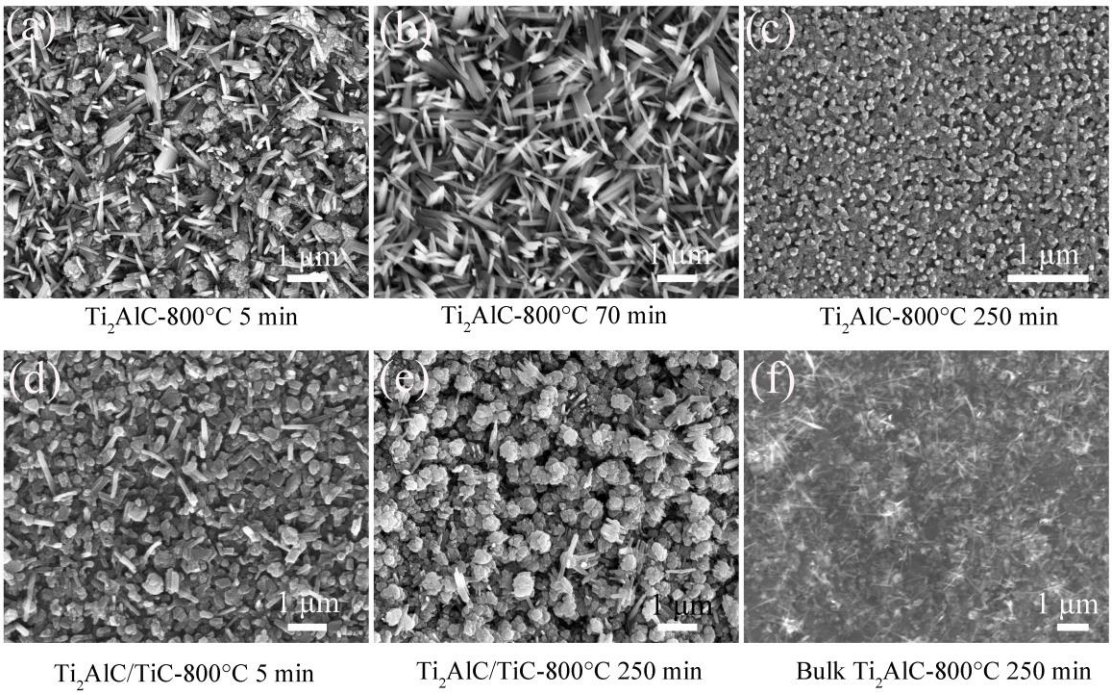

Fig.10 SEM images of typical surface morphologies of Ti_2AlC- and Ti_2AlC/TiC-coated Zry-4 after oxidation at 800°C in steam with different times. The image of bulk Ti_2AlC is also shown as reference.

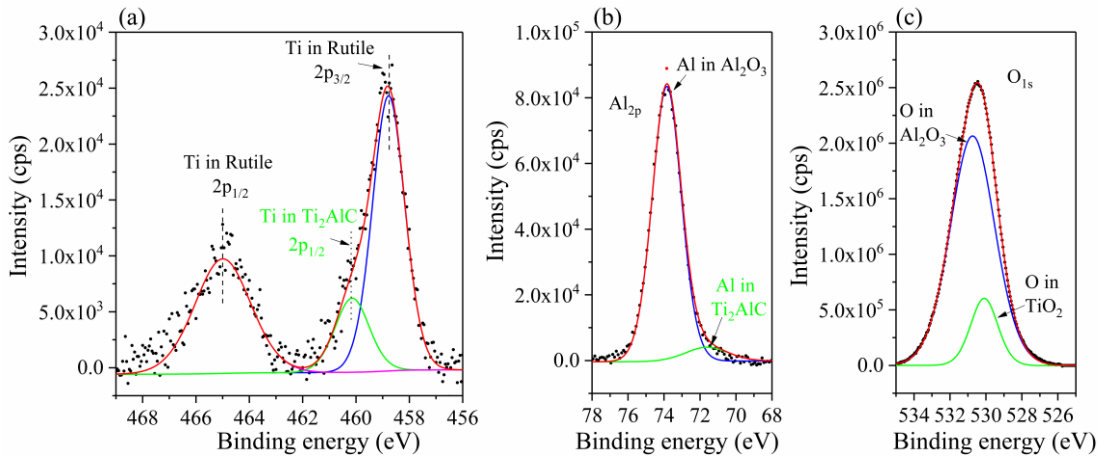

Fig.11 XPS spectra of Ti_2AlC/TiC coating on Zry-4 substrate after oxidation at 800°C for 5 min in steam. (a) Ti, (b) Al, (c) O.

Fig.12 shows the cross sections of the coatings after oxidation at 800°C in steam for 5 min with corresponding EDS elemental mapping and line scanning profiles. Different oxide layer arrangements were observed for the coatings with and without TiC barrier. For the coatings without barrier, the oxide scale demonstrated a double-layered structure. The surface oxide layer was Al_2O_3-rich with certain amount of TiO_2 followed by a TiO_2 layer with trace of Al_2O_3 beneath as shown in Fig.12a and separated by the dashed lines. The Al_2O_3-rich layer was relatively denser compared to the TiO_2 layer. Only one Al_2O_3-rich layer was observed for the coating with TiC barrier (Fig.12b). The total thickness of the oxide layer on the Ti_2AlC coating was around 3 times

thicker than that on the Ti_2AlC/TiC coating. Diffusion of Al from the coatings into the Zry-4 substrate was seen for both coatings; however, the diffusion for the coating without TiC barrier was much more pronounced than that of with barrier as in Fig.12c. The Al diffusion layer exceeded 2 μm for the Ti_2AlC coatings, whereas it was hardly distinguished within thickness below 0.5 μm for the Ti_2AlC/TiC coatings.

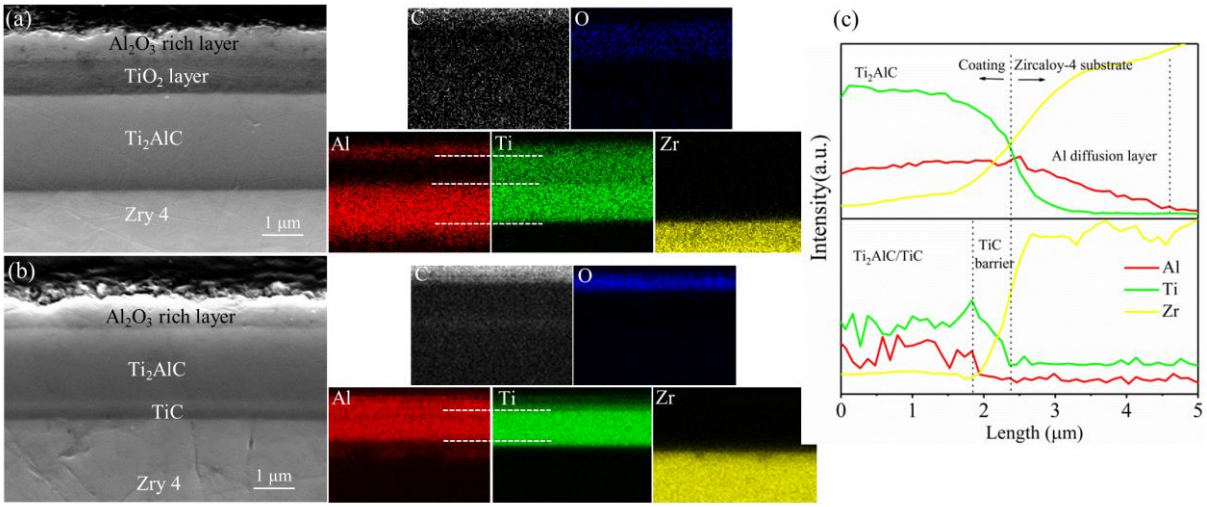

Fig.12 SEM images of cross section of coated samples after oxidation at 800°C in steam for 5 min, (a) Ti_2AlC- and (b) Ti_2AlC/TiC-coated Zry-4 with corresponding EDS elemental mapping; (c) EDS line-scanning profiles at the coating/substrate interfaces.

After 250 min oxidation at 800°C, the bare Zry-4 samples were oxidized forming an oxide layer of around 60 μm thick as shown in Fig.13a with the optical images of typical cross sections. The Ti_2AlC coating without barrier was fully oxidized. Partial spallation of the fully oxidized coating was shown in Fig.13b on the upper side of the sample. The underneath substrate was oxidized on both sides; the oxide layer was significantly thicker (~40 μm) for the side where the coating went lost than that of the other side (~10 μm) where the coating still stayed in touch (Fig.13b). The thinner oxide layer on the undetached area implied that the fully consumed coatings could still act as diffusion barrier to suppress the fast penetration of oxidizing gas into the substrate. It was important to find that the Ti_2AlC/TiC coatings away from the edge maintained intact and adhesive, and was only partially consumed after 250 min oxidation at 800°C as shown in Fig.13c. On the other hand, it can be obviously observed that the uncoated edges of Zry-4 substrate were aggressively oxidized. The steam penetrated into the matrix of the substrate along the edges, leading to the premature failure of the coating at this region. Therefore, the oxidation of uncoated edge areas of Zry-4 substrate (Fig.13.c) is mainly responsible for the slightly faster weight gain rate of Ti_2AlC/TiC-coated Zry-4 compared to bulk Ti_2AlC after 150 min in Fig.8.

The cross sections were also checked by SEM and the images with the EDS elemental mapping are shown in Fig.14. The completely oxidized Ti_2AlC coatings resulted in a three-layered oxide structure (Fig.14a): relatively dense Al_2O_3-rich layers located at the gas/coating interface and the coating/substrate interface separated by a porous TiO_2 layer in the middle, indicating two-direction diffusion of the Al in the coating. The coatings detached form the substrate surface and a gap appeared between the coating and the substrate. The delamination was due to the thermal expansion coefficients mismatch between the completely oxidized coating and substrate during cooling. The oxide layer formed on the Ti_2AlC/TiC coating was similar to that of the Ti_2AlC coating after oxidation for 5 min shown in Fig.12a. The surface was an Al_2O_3-rich layer followed by a porous TiO_2 layer below. However, there was a slight difference observed, i.e. a nearly pure Al_2O_3 layer emerged between the Al_2O_3-rich layer and TiO_2 layer as shown by the mapping. Nearly 2.5 μm thick Ti_2AlC retained after 250 min oxidation. Both the gas/coating interface and the coating/substrate interface became rough, illustrating the outward diffusion of cations and inward diffusion of anions occurred simultaneously. The Al in the Ti_2AlC coating penetrated through the TiC diffusion barrier to obtain a thick diffusion zone during the long exposure, and no obvious diffusion of Ti and Zr was confirmed (Fig.14b).

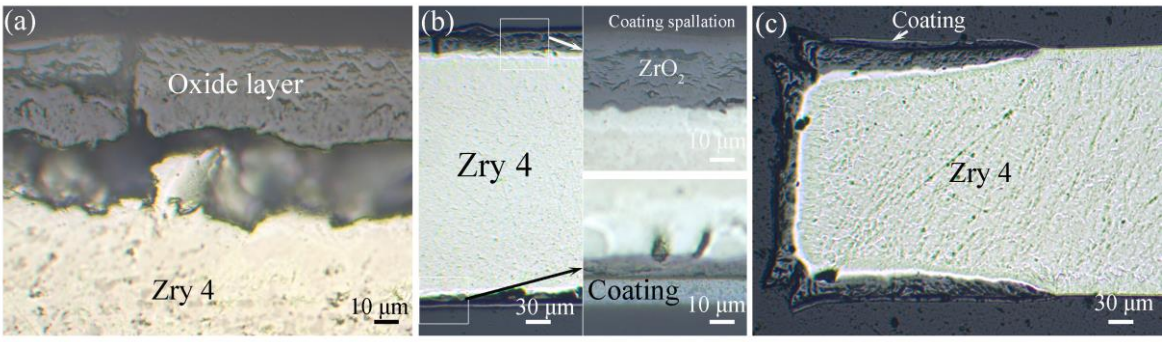

Fig.13 Optical images of typical cross sections after oxidation at 800°C in steam for 250 min (a) Zry-4 substrates, (b) Ti_2AlC- and (c) Ti_2AlC/TiC-coated Zry-4.

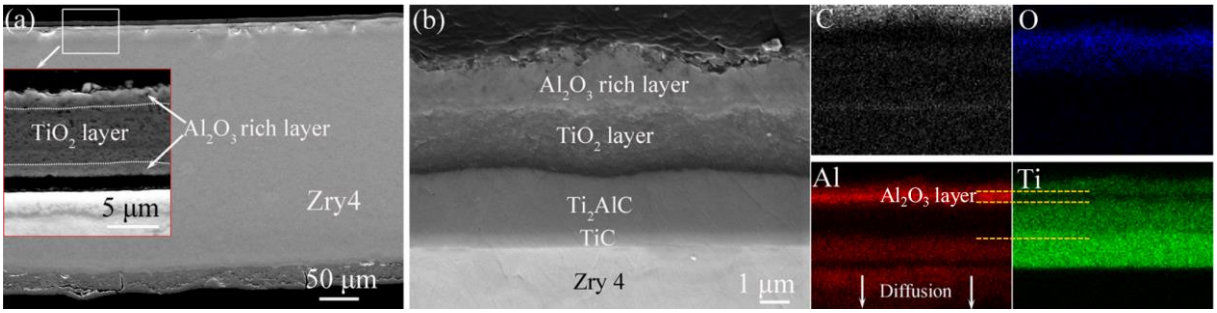

Fig.14 SEM images of cross sections after oxidation at 800°C in steam for 250 min. (a) Ti_2AlC- and (b) Ti_2AlC/TiC-coated Zry-4 with corresponding elemental mapping.

3.2.2. 1000°C and 1200°C oxidation

The oxidation kinetics of the bare and coated Zry-4 at 1000°C and 1200°C in steam were shown in Fig.15. The oxidation rate of the coated Zry-4, both the Ti_2AlC and Ti_2AlC/TiC coatings, did not show any noticeable reduction compared to the uncoated samples. This reflects that the coatings are rapidly oxidized at temperature reaching 1000°C. At 1000°C, the oxidation kinetics of polished Zry-4 first obeyed a parabolic law, and then transferred to a linear law at around 150 min. The transition is caused by so-called breakaway well known for zirconium alloys at temperatures below 1050°C [33]. The later transition compared with literature results, e.g. [34], may be due to the polished surfaces of the samples used in this study. The sample was observed to be fully oxidized at around 240 min (Fig.15a) and the weight gain then remained constant. However, the oxidation kinetics of coated Zry-4 samples followed a parabolic law during the whole exposure up to 250 min. The coated samples demonstrated slightly improved oxidation resistance and were not completely oxidized, mainly due to the delay or, for the Ti_2AlC/TiC coating absence of the transition to breakaway. Oxidation at 1200°C resulted in a parabolic law for both the bare and coated Zry-4 samples. The weight gain of the coating with TiC barrier (40.9 mg/cm^2) was slightly lower than that of without barrier (48.7 mg/cm^2) at the end of 15 min exposure (Fig.15b). Different from the coatings, bulk Ti_2AlC demonstrated an extremely low weight gain (1.06 mg/cm^2 - 250 min oxidation at 1200°C), almost two magnitudes lower than that of coated samples. The weight gain at 1200°C was even lower than that at 1000°C (1.47 mg/cm^2), suggesting that high-temperature oxidation of bulk Ti_2AlC promoted the selective oxidation of Al to form a protective α-Al_2O_3 scale [16].

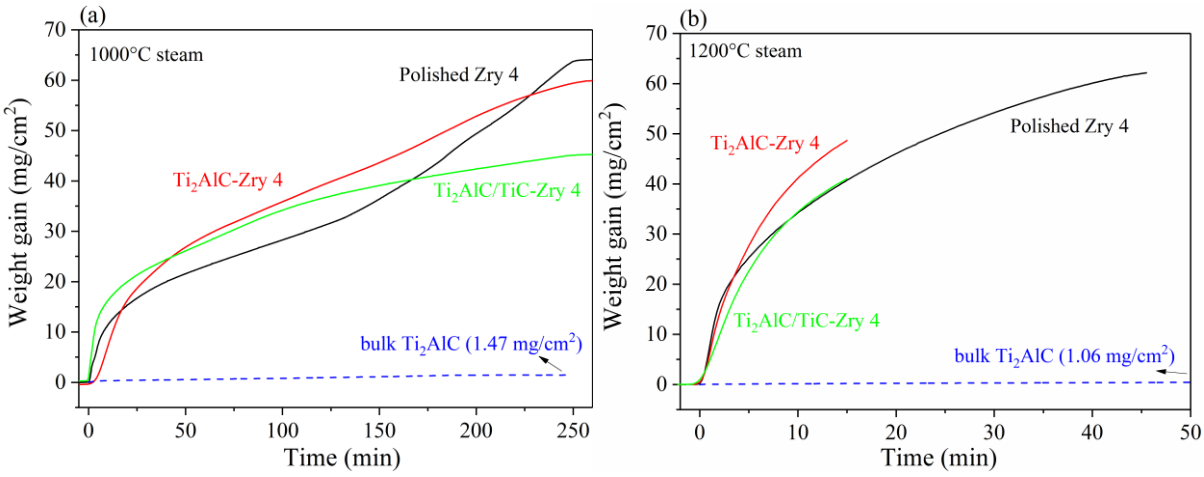

Fig.15 Oxidation kinetics of bulk Ti_2AlC, polished Zry-4 substrates, and Ti_2AlC- and Ti_2AlC/TiC-coated Zry-4 at (a) 1000°C and (b) 1200°C in steam.

The optical images of cross sections of coated Zry-4 after oxidation in steam at 1000°C for 5 min and at 1200°C for 15 min are shown in Fig.16. Fig.16a and b clearly reveal the full consumption of the coatings even just after oxidation at 1000°C for 5 min. The underneath Zry-4 substrates were seriously attacked by steam resulting in a porous, cracked and hence non-protective ZrO_2 layer. The Ti_2AlC-coated Zry-4 sample was almost fully consumed after oxidation at 1200°C for 15 min as in Fig.16c. The sample fractured into two pieces due to two-side oxidation. The coating with TiC barrier demonstrates better oxidation resistance as an unconsumed metal layer is clearly seen.

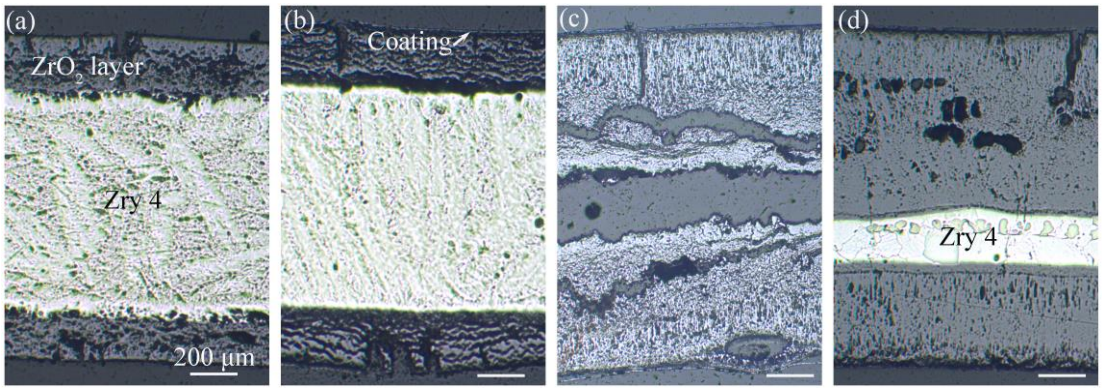

Fig.16 Optical images of cross sections of (a) Ti_2AlC- and (b) Ti_2AlC/TiC- coated Zry-4 after oxidation at 1000°C for 5 min, (c) Ti_2AlC- and (d) Ti_2AlC/TiC- coated Zry-4 after oxidation at 1200°C for 15 min.

3.2.3. Ramp steam oxidation

In order to determine the initial failure temperature of the coatings in steam, ramp transient oxidation tests from 300 to 1000°C were performed simulating typical LOCA scenario. Fig.17 shows the weight gain of polished Zry-4 substrates, Ti_2AlC- and Ti_2AlC/TiC-coated Zry-4 during the ramp tests with 10 K/min heating rate. The initial failure temperature is defined as the transition point in the oxidation kinetics at which the samples suffered accelerated oxidation rate. The dotted lines are plotted as a guidance to show how the temperatures are found. The corresponding weight gains are all around 2 mg/cm^2 at the transition point. The temperature values were obtained by drawing a vertical dotted line from the weight gain curves at the transition point and reading the temperature from its intersection with the temperature profile, as in Fig.17 for the uncoated sample. A continuously increasing oxidation rate, especially beyond 700°C, due to the strong temperature dependence of oxidation of the samples can be seen. Meanwhile, the bare Zry-4 showed much faster oxidation rate compared to the coated samples during the test. The temperature at which bare Zry-4 underwent accelerated oxidation rate was found to be around 810°C. The accelerated oxidation rate of Ti_2AlC-coated Zry-4 started from about 930°C, more than 100°C higher than that of bare Zry-4. The performance of the coating

with TiC barrier was further slightly improved, the initial failure temperature reaching 960°C. The observations were consistent with the isothermal oxidation results, in which the coatings showing weak or no protective effect beyond 1000°C. It is necessary to mentation that the performance of the coatings during such transient test can be strongly dependent on the heating rate. The results obtained here are only valid for the applied heating rate of 10 K/min.

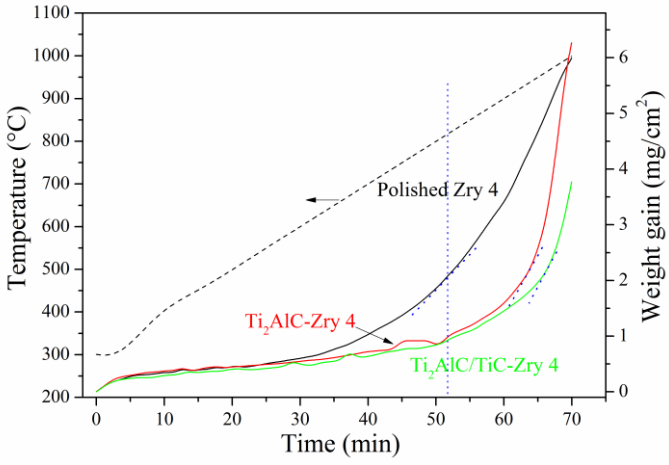

Fig.17 Weight gain of polished Zry-4 substrates, and Ti_2AlC- and Ti_2AlC/TiC-coated Zry-4 during ramp test from 300°C to 1000°C in steam.

4. Discussion

Even though phase-pure and dense Ti_2AlC coatings were successfully obtained in this study, the superior oxidation resistance of bulk Ti_2AlC was not inherited by the magnetron-sputtered coatings. The coatings presented distinctive and more complex oxidation behavior compared to bulk MAX phase materials. Oxidation of bulk Ti_2AlC at temperature below 700°C leads to an anomalous oxidation with relatively high kinetics due to the formation of un-protective scales consisting of anatase and rutile [30]. The oxide scale changes to a two-layer structure: an outer TiO_2 (rutile) layer with alumina inclusion and an inner alumina layer with increasing oxidation temperature. Transition alumina phases of γ-, θ- Al_2O_3 mainly grow at temperature lower than 900°C; high-temperature oxidation promotes the growth of a dense, adherent α-Al_2O_3 layer above the bulk. The Ti_2AlC coatings without TiC barrier in this study also form a scale with two sublayers before being completely consumed after oxidation at intermediate temperature (800°C). However, contrary to the scale formed on the bulk, the surface layer is an Al_2O_3-rich layer mixed with TiO_2 and the inner porous layer is TiO_2 (rutile) with traces of Al_2O_3. One slight difference for the coatings with TiC barrier is that a nearly pure alumina layer is detected between these two layers after oxidation at the same temperature.

The oxidation mechanism for the growth of a double-layer scale on the surface of bulk Ti_2AlC can be explained by the initial transient oxidation, and subsequent selective oxidation of Al [16,35]. Hence, it is reasonable to propose that similar oxidation sequences also occur for the Ti_2AlC coatings. The distinct scaling behavior of coatings can be attributed to various factors, like microstructure and thickness of the coatings as well as the interaction between the coating and the substrate. At the initial stage of oxidation, both TiO_2 and Al_2O_3 can simultaneously nucleate on the surface of the samples. Even though the formation of Al_2O_3 is thermodynamically favored, it has been proved that the growth kinetics of TiO_2 is much faster than that Al_2O_3 at low temperature and high oxidant partial pressure [35]. The grains are usually coarse in Ti_2AlC bulk ceramic. On the contrary, it has been demonstrated that the coatings obtained in this study are nanocrystalline with an abundance of grains and boundaries. As a result, TiO_2 will grow preferentially on the surface of bulk Ti_2AlC as Ti represents the main constituent. In terms of coating, the outward diffusion of Al is supposed to be considerably enhanced due to the numerous grain boundaries as well as the unique layered structure of MAX phases resulting in fast migration rate of the A elements [36]. The grain sizes of the oxide formed on the Ti_2AlC/TiC coatings are found to be much larger than that on the bulk Ti_2AlC after oxidation at same conditions as shown in Fig.10e and f, which confirms the explanation. Therefore, an Al_2O_3-rich layer grows on the surface of Ti_2AlC coating during the transient oxidation stage.

Continued oxidation will decrease the oxidant partial pressure at the scale/substrate interface, promoting the selective oxidation of Al due to a much lower oxygen pressure needed for the formation of alumina. The bulk Ti_2AlC can act as an Al reservoir to provide adequate aluminum for producing a continuous Al_2O_3 layer. For alumina-forming materials, breakaway oxidation occurs once the Al content is below the critical minimum aluminum content due to the continuing consumption of the Al, resulting in a catastrophic breakaway oxidation by formation of non-protective matrix-based scales. This phenomenon has been well documented for FeCrAl-based alloys [37]. Recently the breakaway oxidation of Ti_3AlC_2 MAX phase (Ti_2AlC counterpart) at 1100°C in air has been investigated, and the corresponding critical Al content is proved to be around 6% lower than the initial content [38]. The specimen thickness has a profound effect on the time to breakaway oxidation; longer service time can be achieved by increasing the thickness to supply more Al. Fast diffusion of Al from the Ti_2AlC coating without TiC diffusion barrier into the substrate (Fig.12a) quickly reduce the Al content in the coating, probably rapidly leading to the lower Al contents than the corresponding critical ones for selective oxidation of Al in Ti_2AlC coatings. Consequently, further oxidation also produces mixed oxides of Al_2O_3 and TiO_2. For the Ti_2AlC/TiC coatings, even though the diffusion of Al into the substrate is unavoidable,

the diffusion rate is suppressed by the presence of the TiC barrier. The relatively high Al content in the Ti_2AlC/TiC coatings enables successful establishment of a pure Al_2O_3 layer beneath the transient oxide layer (Fig.14b), resulting in lower oxidation rate and better oxidation resistance than Ti_2AlC coatings. The formation of an inner porous TiO_2 layer can be understood by two steps: (1) two direction outward diffusion of Al from the coatings probably firstly leave a metastable Ti_2C layer beneath the oxide scale; (2) inward diffusion of the oxidant through the Al_2O_3-rich layer oxidizes the Ti_2C layer to form firstly TiC_xO_{1-x} [39], then TiO_2 and carbon oxides gases as following overall equations:

$$Ti_2C(s) + 5H_2O(g) = 2TiO_2 \text{ (rutile, s)} + 5H_2(g) + CO(g) \quad (1)$$

$$Ti_2C(s) + 6H_2O(g) = 2TiO_2 \text{ (rutile, s)} + 6H_2(g) + CO_2(g) \quad (2)$$

The Al-depleted hexagonal unit can shrink accompanied by a large reduction of volume and the Ti_2C slabs can relax to form stable TiC_x (x = 0.97- 0.47) before oxidation as observed during the decomposition of Ti_3SiC_2 thin film [40]. Oxidation of TiC at high temperature also produce a porous TiO_2 scale [41], hence, it can be expected that the inner TiO_2 layer was less dense and contained voids.

The driving forces for two-direction diffusion of Al can be interpreted by thermodynamic stability of various oxides and chemical potential of Al at the interfaces. As known by the experimental results, steam (or oxygen) and aluminum are the main diffusing components during the formation of the sub-layered oxide scale. The Gibbs free energy of formation of TiO_2 and Al_2O_3 per mole oxygen at 1073 K (800°C) is -749.8 kJ/mol and -891.5 kJ/mol. In addition, in Ti_2AlC MAX phases the covalent Ti-C bonds, similar to those in the TiC compound, are much stronger than the metallic-like Ti-Al bonds, resulting in relatively high chemical activity and fast migration rate of Al atoms [14]. Due to the more negative value of Gibbs free energy of formation of Al_2O_3 and the mobility of aluminum atoms in the coatings, surface oxidation thus drives Al outwardly towards to the coating-ambient interface. The progressively decreasing oxidant partial pressure over the coating layer promotes the selective oxidation of Al. In addition, it seems that the aluminum atoms can diffuse through the porous TiO_2 layer, and then precipitate as alumina beneath the scale formed during the transient oxidation stage (Fig.14b). Similar behavior has been reported previously for the oxidation of bulk Ti_3AlC_2, $Ti_2AlC_{0.5}N_{0.5}$ [42], and Ti_2AlN [43]. One explanation is that the relatively low oxidation temperature (800°C here) decreases the reaction kinetics between the outward aluminum cations and inward oxidant anions providing the aluminum cations time to migrate out [36]. Chemical potential gradients are the driving forces for inward diffusion of Al from the coatings into the substrate. The high chemical

activity of Al at the Ti_2AlC coating side and high solubility of Al in zirconium contribute to inward diffusion and alloying of Al with the Zircaloy-4 substrate. The strong covalent Ti-C bonds combined with low solubility of Al in the TiC barrier obviously raise the activation energy of Al diffusion and thus reduce the inward diffusion rate [44]. Fig.18 presents the schematic view of microstructural evolution from the surface to the substrate during oxidation at 800°C in steam, based on the scaling behavior and scaling evolution. The main difference between the coatings with and without barrier is the non-establishment of a continuous pure alumina layer for the coatings without TiC barrier due to fast diffusion of Al from the coatings into the substrate.

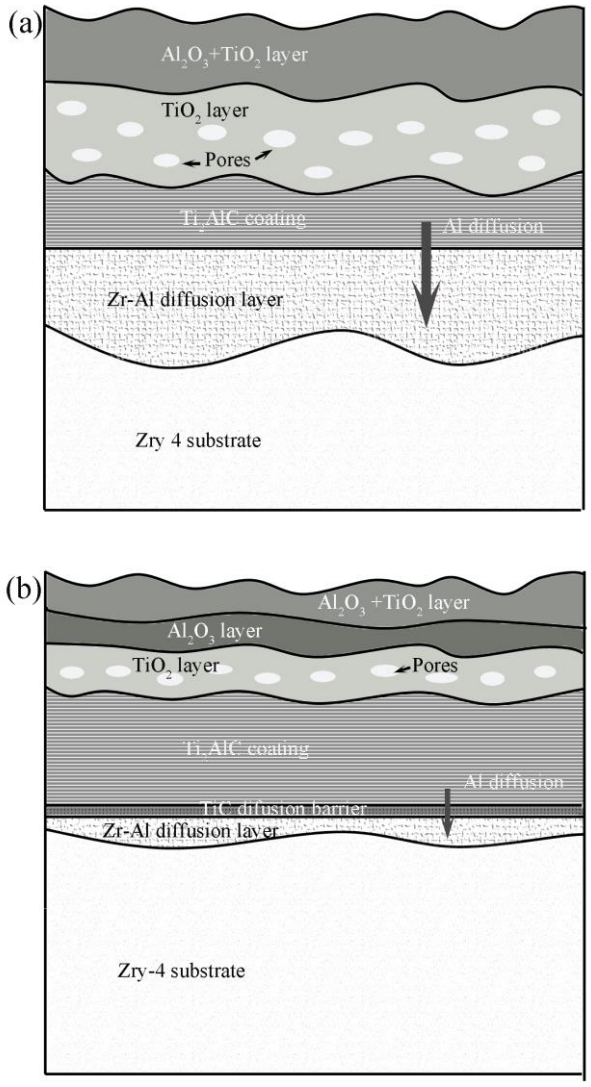

Fig.18 Schematic of cross sectional microstructure of (a)Ti_2AlC and (b)Ti_2AlC/TiC coating on Zry-4 during oxidation at 800°C in steam with 5.5 μm thick coatings.

Fig.19 shows the diffusion coefficients of steam and oxygen in α-Al_2O_3 along with that of Al in various bulk materials as a function of temperature. Water vapor is usually more aggressive than oxygen, and the diffusion rate of water in α-Al_2O_3 is several magnitudes faster than that of

oxygen [45]. Preferred transient oxides grow in water vapor conditions has been found compared to in air for alumina-forming materials oxidized at low temperatures. Steam can also stabilize the transition alumina inhibiting the phase transformation to stable α-Al_2O_3 [46,47]. Hence, it can be expected that the oxidation of the coatings at 800°C for 250 min in steam contribute to the growth of metastable θ-Al_2O_3. The transition alumina shows less protective effect compared to α-Al_2O_3 with higher diffusivity of the oxidant [48]. Therefore, the steam can readily penetrate through the transition alumina layer to oxidize the remaining Ti_2C layer after loss of Al.

With the temperature increasing to 1000°C, both the oxidation rate and the inward diffusion of Al into the substrate become much faster. Pantano et.al demonstrated that a minimum coating thickness of about 90 micrometers was needed for cold sprayed Ti_2AlC coatings to be protective against zirconium alloy oxidation at 1200°C in steam [20]. A process that would yield a denser coating would reduce this minimum thickness. Moreover, localized ZrO_2 regions often develop at the coating-substrate interface as a result of diffusion of steam through pores due to the porous structure of sprayed coatings [19,20]. Dense and uniform Ti_2AlC coatings were successfully synthesized by adopting a unique two-step process herein and no internal oxidation of the substrate was confirmed before complete oxidation of the coatings in this study. However, the coatings investigated here are only 5 μm thick; hence, only a limited amount of Al can be supplied. The coatings are supposed to be rapidly consumed during the transient oxidation stage beyond 1000°C due to the low thickness. In addition, the fast failure of the coatings may be partly attributed to the high oxygen/steam affinity of Zry-4 at this high temperature allowing fast steam diffusion into the substrate along the uncoated edges as shown in Fig.13c. The phase transformation of Zircaloy-4 substrates at around 860°C presumably induces additional thermal and internal stresses at the coating/substrate interface. These effects, in turn, cause the cracking and failure of the coatings. Generally speaking, the 5 μm Ti_2AlC/TiC coating here can provide sufficient protection of the Zry-4 substrate from fast attack by steam at 800°C, or maybe 900°C even considering the edge effect as shown in the ramp test. For higher temperature application during severe accident scenarios, thicker coatings and an appropriate diffusion barrier are needed as discussed above.

One of the key reasons contributing to the excellent high-temperature oxidation resistance of Ti_2AlC and Ti_3AlC_2 MAX phase is their unique nanolaminated microstructure where the $Ti_{n+1}C_n$ layers being interleaved with single Al layers. As explained before, relatively weak metallic-like Ti-Al bonds leads to high chemical activity and fast migration rate of Al atoms in $Ti_{n+1}AlC_n$ MAX phases. Despite containing only 16.67 at.% Al, Ti_3AlC_2 MAX phase can form a protective Al_2O_3 scale during high-temperature oxidation by selective oxidation of Al. Fig.19 also compares the

diffusion coefficient of Al in Ti_2AlC [49], Ti_3AlC_2 [50] and other common alumina-forming materials Fe(Al) [44], TiAl [51] and NiAl alloys [52]. It can be clearly seen that the diffusion rate of Al in MAX phase is around 2-5 magnitudes higher than that in these alloys.

The inward diffusion rate of Al from the Ti_2AlC coating into the substrate in this study at 800°C was estimated to be an order of magnitude 10^{-13} $m^2 \cdot s$ according to the depth profile of Al after annealing and short time oxidation, which is in the same order of magnitude compared to previous studies using diffusion couples [49]. For the coatings with TiC barrier, the diffusion rate decreased by around one magnitude. It is necessary to mention here that this advantage can become a challenge for application of $Ti_{n+1}AlC_n$ MAX phases as oxidation resistant coatings on some practical substrates, especial alloys. The fast inward diffusion of Al into the substrate leads to the loss of the Al reservoir and also may degrade the properties of the substrate [53,54]. The 500 nm thick TiC diffusion barrier used in this study can inhibit the rapid migration of Al to some extent at 800°C, but not sufficiently. An appropriate and effective diffusion barrier is needed to further improve the MAX phase coatings performance for high-temperature applications during severe accidents.

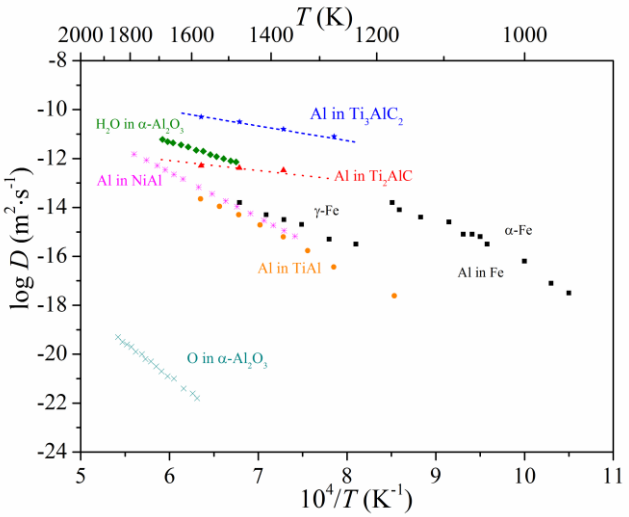

Fig.19 Diffusion coefficients of Al in various bulk materials along with steam and oxygen in α-Al_2O_3 as a function of temperature. Al in Fe(Al) [44], Ti_2AlC [49], Ti_3AlC_2 [50], TiAl [51] and NiAl alloys [52]. H_2O and O in α-Al_2O_3 [45].

5. Conclusions

Ti_2AlC MAX phase coatings (5.5 μm thickness) with or without 500 nm TiC diffusion barrier have been synthesized and evaluated with respect to their capability of protecting Zircaloy-4 substrate from fast oxidation in high-temperature steam. Dense and phase-pure Ti_2AlC coatings were obtained by non-reactive magnetron sputtering of elemental multilayer thin films from three

element targets, and subsequent thermal annealing in argon at 800°C for 10 min. The coatings, around 15 GPa of hardness and 200 GPa of modulus, were much stiffer than the Zircaloy-4 substrate and displayed a brittle failure mode in scratch tests. The Ti_2AlC coatings without diffusion barrier possess higher interfacial adhesion strength thanks to formation of a strong metallurgical bond at the coating/substrate interface.

The coated samples followed parabolic oxidation kinetics and demonstrated significant improvement of oxidation resistance compared to bare Zircaloy-4 at 800°C in steam. The Ti_2AlC coatings without TiC barrier formed an oxide scale overlayer consisting of two sublayers: an outer metastable θ-Al_2O_3 rich layer mixed with TiO_2 (rutile) and an inner porous TiO_2 layer with traces of Al_2O_3; correspondingly, a triple-layered scale (θ-Al_2O_3+TiO_2/θ-Al_2O_3/TiO_2) grew on coatings with barrier at 800°C. The TiC barrier suppressed the rapidly inward diffusion of Al from the coatings into the substrate, contributing to different scale configuration, better oxidation performance and longer life of Ti_2AlC/TiC coatings. Both coatings were rapidly oxidized and showed only a slightly protective effect from around 1000°C. It is suggested that thicker coatings and an appropriate diffusion barrier are needed for high temperature application beyond 1000°C.

Acknowledgment

This work was supported by the Helmholtz (HGF) programs NUSAFE and STN at the Karlsruhe Institute of Technology. It was further partially carried out with support of the Karlsruhe Nano Micro Facility (KNMF, www.knmf.kit.edu), a Helmholtz research infrastructure at the Karlsruhe Institute of Technology (KIT, www.kit.edu). C. Tang and X. Yu appreciate the PhD fellowship funded by the China Scholarship Council (CSC). The authors also thank the Mr. S. Zils for technical support during coating deposition, Dr. A. Jianu for providing the bulk Ti_2AlC specimens and Dr. J. Ye for support of scratch tests.

References

[1] International Atomic Energy Agency, IAEA Annual Report 2014, 2014.

[2] S.J. Zinkle, G.S. Was, Materials challenges in nuclear energy, Acta Mater. 61 (2013) 735–758.

[3] T.R. Allen, R.J.M. Konings, A.T. Motta, Corrosion of Zirconium Alloys, in: Rudy J.M. Konings (Ed.), Compr. Nucl. Mater., Elsevier Ltd, 2012: pp. 49–68.

[4] M. Steinbrück, M. Große, L. Sepold, J. Stuckert, Synopsis and outcome of the QUENCH experimental program, Nucl. Eng. Des. 240 (2010) 1714–1727.

[5] M. Hirano, T. Yonomoto, M. Ishigaki, N. Watanabe, Y. Maruyama, Y. Sibamoto, et al., Insights from review and analysis of the Fukushima Dai-ichi accident, J. Nucl. Sci. Technol. 49 (2012) 1–17. doi:10.1080/18811248.2011.636538.

[6] S.M. Bragg-Sitton, Development of advanced accident- tolerant fuels for commercial LWRs, Nucl. News. 53 (2014) 83–91.

[7] S.J. Zinkle, K.A. Terrani, J.C. Gehin, L.J. Ott, L.L. Snead, Accident tolerant fuels for LWRs: A perspective, J. Nucl. Mater. 448 (2014) 374–379.

[8] B.A. Pint, K.A. Terrani, Y. Yamamoto, L.L. Snead, Material Selection for Accident Tolerant Fuel Cladding, Metall. Mater. Trans. E. 2 (2014) 190–196.

[9] E. Alat, A.T. Motta, R.J. Comstock, J.M. Partezana, D.E. Wolfe, Ceramic coating for corrosion (c3) resistance of nuclear fuel cladding, Surf. Coatings Technol. 281 (2015) 133–143.

[10] J.-H. Park, H.-G. Kim, J. Park, Y.-I. Jung, D.-J. Park, Y.-H. Koo, High temperature steam-oxidation behavior of arc ion plated Cr coatings for accident tolerant fuel claddings, Surf. Coatings Technol. 280 (2015) 256–259.

[11] C. Tang, M. Stueber, H.J.H.J. Seifert, M. Steinbrueck, Protective coatings on zirconium-based alloys as accident-tolerant fuel (ATF) claddings, Corros. Rev. 35 (2017) 141–166.

[12] J.C. Brachet, M. Le Saux, M. Le Flem, S. Urvoy, E. Rouesne, T. Guilbert, et al., On-going studies at CEA on chromium coated zirconium based nuclear fuel claddings for enhanced Accident Tolerant LWRs Fuel, in: LWR Fuel Performance/TopFuel/WRFPM, Zurich, Switzerland, 2015: pp. 31–38.

[13] R. Van Nieuwenhove, K. Daub, H. Nordin, R. Van Nieuwenhove, H. Nordin, Investigation of the impact of coatings on corrosion and hydrogen uptake of Zircaloy-4, J. Nucl. Mater. 467 (2015) 260–270.

[14] M.W. Barsoum, The MN+1AXN phases: a new class of solids; thermodynamically stable nanolaminates, Prog. Solid State Chem. 28 (2000) 201–281.

[15] J.L. Smialek, Diffusivity in Alumina Scales Grown on Al-MAX Phases, Corros. Sci. 91 (2014) 1–10. doi:10.1016/j.corsci.2014.11.030.

[16] D.J. Tallman, B. Anasori, M.W. Barsoum, A Critical Review of the Oxidation of Ti2AlC, Ti3AlC2 and Cr2AlC in Air, Mater. Res. Lett. 1 (2013) 115–125.

[17] D.J. Tallman, E.N. Hoffman, E.N. Caspi, B.L. Garcia-diaz, G. Kohse, R.L. Sindelar, et al., Effect of neutron irradiation on select MAX phases, Acta Mater. 85 (2015) 132–143.

[18] C. Tang, M. Steinbrück, M. Große, T. Bergfeldt, H.J. Seifert, Oxidation behavior of Ti2AlC in the temperature range of 1400 °C–1600 °C in steam, J. Nucl. Mater. 490 (2017) 130–142.

[19] B.R. Maier, B.L. Garcia-Diaz, B. Hauch, L.C. Olson, R.L. Sindelar, K. Sridharan, Cold spray deposition of Ti2AlC coatings for improved nuclear fuel cladding, J. Nucl. Mater. 466 (2015) 712–717.

[20] M. Pantano, V. Avincola, P.A. De Seze, T. McKrell, M.S. Kazimi, High temperature steam oxidation performance of MAX phase (Ti2AlC) coated ZIRLO, in: Int. Congr. Adv. Nucl. Power Plants, ICAPP 2014, American Nuclear Society, 2014: pp. 2126–2135.

[21] H. Yeom, B. Hauch, G. Cao, B. Garcia-Diaz, M. Martinez-Rodriguez, H. Colon-Mercado, et al., Laser surface annealing and characterization of Ti2AlC plasma vapor deposition coating on zirconium-alloy substrate, Thin Solid Films. 615 (2016) 202–209..

[22] C. Tang, M. Klimenkov, U. Jaentsch, H. Leiste, M. Rinke, S. Ulrich, et al., Synthesis and characterization of Ti2AlC coatings by magnetron sputtering from three elemental targets and ex-situ annealing, Surf. Coatings Technol. 309 (2017) 445–455.

[23] O.D. Leaffer, S. Gupta, M.W. Barsoum, J.E. Spanier, On Raman scattering from selected M2 AC compounds, J. Mater. Res. 22 (2011) 2651–2654.

[24] V. Presser, M. Naguib, L. Chaput, A. Togo, G. Hug, M.W. Barsoum, First-order Raman scattering of the MAX phases: Ti2AlN, Ti2AlC0.5N0.5, Ti2AlC, (Ti0.5V0.5)2AlC, V2AlC, Ti3AlC2, and Ti3GeC2, J. Raman Spectrosc. 43 (2012) 168–172.

[25] A. Ferrari, J. Robertson, Interpretation of Raman spectra of disordered and amorphous carbon, Phys. Rev. B. 61 (2000) 14095–14107.

[26] A. Abdulkadhim, M. to Baben, T. Takahashi, V. Schnabel, M. Hans, C. Polzer, et al., Crystallization kinetics of amorphous Cr2AlC thin films, Surf. Coatings Technol. 206 (2011) 599–603.

[27] J. Wang, Y. Zhou, Z. Lin, F. Meng, F. Li, Raman active phonon modes and heat capacities of Ti2AlC and Cr2AlC ceramics: first-principles and experimental investigations, Appl. Phys. Lett. 86 (2005) 101902/1-101902/3.

[28] J. Robertson, Diamond-like amorphous carbon, Mater. Sci. Eng. R Reports. 37 (2002) 129–281.

[29] S. Suman, M.K. Khan, M. Pathak, R.N. Singh, Investigation of elevated-temperature mechanical properties of δ-hydride precipitate in Zircaloy-4 fuel cladding tubes using nanoindentation, J. Alloys Compd. 726 (2017) 107–113.

[30] X. Wang, Y. Zhou, Intermediate-temperature oxidation behavior of Ti2AlC in air, J. Mater. Res. (2002) 2974–2981.

[31] S.R.J. Saunders, M. Monteiro, F. Rizzo, The oxidation behaviour of metals and alloys at high temperatures in atmospheres containing water vapour: A review, Prog. Mater. Sci. 53 (2008) 775–837.

[32] K. Djebaili, Z. Mekhalif, A. Boumaza, A. Djelloul, XPS, FTIR, EDX, and XRD analysis of Al2O3 scales grown on PM2000 alloy, J. Spectrosc. 2015 (2015) 6670–6683.

[33] M. Steinbrück, M. Grosse, Deviations From Parabolic Kinetics During Oxidation of Zirconium Alloys, in: Zircon. Nucl. Ind. 17th Vol., ASTM International, 100 Barr Harbor Drive, PO Box C700, West Conshohocken, PA 19428-2959, 2015: pp. 979–1001.

[34] M. Steinbrück, N. Vér, M. Große, Oxidation of advanced zirconium cladding alloys in steam at temperatures in the range of 600-1200 °C, Oxid. Met. 76 (2011) 215–232.

[35] J.L. Smialek, Kinetic Aspects of Ti2AlC MAX Phase Oxidation, Oxid. Met. 83 (2015) 351–366.

[36] J. Frodelius, J. Lu, J. Jensen, D. Paul, L. Hultman, P. Eklund, Phase stability and initial low-temperature oxidation mechanism of Ti2AlC thin films, J. Eur. Ceram. Soc. 33 (2013) 375–382.

[37] I. Gurrappa, S. Weinbruch, D. Naumenko, W.J.J. Quadakkers, Factors governing breakaway oxidation of FeCrAl-based alloys, Mater. Corros. 51 (2000) 224–235.

[38] X. Li, L. Zheng, Y. Qian, J. Xu, M. Li, Breakaway oxidation of Ti3AlC2 during long-term exposure in air at 1100°C, Corros. Sci. 104 (2016) 112–122.

[39] M. Gherrab, V. Garnier, S. Gavarini, N. Millard-Pinard, S. Cardinal, Oxidation behavior of nano-scaled and micron-scaled TiC powders under air, Int. J. Refract. Met. Hard Mater. 41 (2013) 590–596.

[40] J. Emmerlich, D. Music, P. Eklund, O. Wilhelmsson, U. Jansson, J.M. Schneider, et al., Thermal stability of Ti3SiC2 thin films, Acta Mater. 55 (2007) 1479–1488.

[41] A. Onuma, H. Kiyono, S. Shimada, M. Desmaison, High temperature oxidation of sintered TiC in an H2O-containing atmosphere, Solid State Ionics. 172 (2004) 417–419.

[42] M.W. Barsoum, N. Tzenov, A. Procopio, T. El-Raghy, M. Ali, Oxidation of Tin+1AlXn (n=1-3 and X=C, N): II. Experimental Results, J. Electrochem. Soc. 148 (2001) C551.

[43] B. Cui, R. Sa, D.D. Jayaseelan, F. Inam, M.J. Reece, W.E. Lee, Microstructural evolution during high-temperature oxidation of spark plasma sintered Ti2AlN ceramics, Acta Mater. 60 (2012) 1079–1092.

[44] G. Neumann, C. Tuijn, Self-diffusion and Impurity Diffusion in Pure Metals: Handbook of Experimental Data, Elsevier, 2011.

[45] R.H. Doremus, Diffusion in alumina, J. Appl. Phys. 100 (2006) 101301.

[46] S. Canovic, J. Engkvist, F. Liu, H. Lai, H. Götlind, K. Hellström, et al., Microstructural Investigation of the Initial Oxidation of the FeCrAlRE Alloy Kanthal AF in Dry and Wet O2 at 600 and 800°C, J. Electrochem. Soc. 157 (2010) C223.

[47] K. Onal, M.C. Maris-Sida, G.H. Meier, F.S. Pettit, Water vapor effects on the cyclic oxidation resistance of alumina forming alloys, Mater. High Temp. 20 (2003) 327–337.

[48] H.J. Grabke, Oxidation of NiAl and FeAl, Intermetallics. 7 (1999) 1153–1158.

[49] D.J. Tallman, J. Yang, L. Pan, B. Anasori, M.W. Barsoum, Reactivity of Zircaloy-4 with Ti3SiC2 and Ti2AlC in the 1100–1300°C temperature range, J. Nucl. Mater. 460 (2015) 122–129.

[50] X.H. Wang, F.Z. Li, J.X. Chen, Y.C. Zhou, Insights into high temperature oxidation of Al2O3-forming Ti3AlC2, Corros. Sci. 58 (2012) 95–103.

[51] Y. Mishin, C. Herzig, Diffusion in the Ti–Al system, Acta Mater. 48 (2000) 589–623.

[52] R. Nakamura, K. Takasawa, Y. Yamazaki, Y. Iijima, Single-phase interdiffusion in the B2 type intermetallic compounds NiAl, CoAl and FeAl, Intermetallics. 10 (2002) 195–204.

[53] Z. Feng, P. Ke, Q. Huang, A. Wang, The scaling behavior and mechanism of Ti2AlC MAX phase coatings in air and pure water vapor, Surf. Coatings Technol. 272 (2015) 380–386.

[54] M. Fröhlich, Investigations on the oxidation behavior of MAX-phase based Ti2AlC coatings on γ-TiAl, in: Strateg. Mater. Comput. Des. Ceram. Eng. Sci. Proc., 2010: pp. 161–169.